# Rationally Designed Integrin $\beta$3 Mutants Stabilized in the High Affinity Conformation*

**Bing-Hao Luo**[‡§1,2], **John Karanicolas**[¶2,3], **Laura D. Harmacek**[‡], **David Baker**[¶], and **Timothy A. Springer**[‡4]

From the ‡Immune Disease Institute and Department of Pathology, Harvard Medical School, Boston, Massachusetts 02115, the §Department of Biological Sciences, Louisiana State University, Baton Rouge, Louisiana 70803, and the ¶Department of Biochemistry and Howard Hughes Medical Institute, University of Washington, Seattle, Washington 98195

**Integrins are important cell surface receptors that transmit bidirectional signals across the membrane. It has been shown that a conformational change of the integrin $\beta$-subunit headpiece (*i.e.* the $\beta$ I domain and the hybrid domain) plays a critical role in regulating integrin ligand binding affinity and function. Previous studies have used coarse methods (a glycan wedge, mutations in transmembrane contacts) to force the $\beta$-subunit into either the open or closed conformation. Here, we demonstrate a detailed understanding of this conformational change by applying computational design techniques to select five amino acid side chains that play an important role in the energetic balance between the open and closed conformations of $\alpha$IIb$\beta$3. Eight single-point mutants were designed at these sites, of which five bound ligands much better than wild type. Further, these mutants were found to be in a more extended conformation than wild type, suggesting that the conformational change at the ligand binding headpiece was propagated to the legs of the integrin. This detailed understanding of the conformational change will assist in the development of allosteric drugs that either stabilize or destabilize specific integrin conformations without occluding the ligand-binding site.**

Allostery is important in the function of many signaling proteins (1), including cell adhesion molecules, such as integrins (2). Integrins are large, heterodimeric molecules that transmit signals bidirectionally across the plasma membrane and regulate many biological functions, including wound healing, cell differentiation, and cell migration. The conformational changes associated with integrin activation and signaling have been studied structurally and functionally (3–8). Integrins bind ligands at an interface between the $\alpha$-subunit $\beta$-propeller domain and the $\beta$-subunit I domain in the integrin headpiece (2). An acidic residue in the ligand coordinates with a $Mg^{2+}$ ion in a metal ion-dependent adhesion site (MIDAS).[5] Remodeling of ligand-binding residues in the $\beta$ I domain is allosterically linked to reorientation at its interface with the hybrid domain.

Crystal structures of integrins have revealed open, liganded (8) and closed, unliganded (3) conformations of the integrin headpiece (Fig. 1). Movement of the $\beta$1-$\alpha$1 and $\beta$6-$\alpha$7 loops, which bind the MIDAS and ADMIDAS (adjacent to MIDAS) metal ions are coupled to movements of the $\alpha$1 and $\alpha$7 helices, which are adjacent to one another. Reshaping to the open conformation, which exhibits high affinity for ligand, is allosterically linked to C-terminal piston-like movement of the $\alpha$7-helix. This linkage is critical for bidirectional propagation of conformational signals between the ligand binding pocket and other integrin domains. The orientation between the $\beta$ I and hybrid domains appears to represent the critical "translator" for converting large scale interdomain rearrangements into local conformational changes within the $\beta$ I domain that regulate affinity for ligand. The piston-like displacement of the $\alpha$7-helix of the $\beta$ I domain in the "open" crystal structure results in complete remodeling of the interface with the hybrid domain (8). Relative to the closed conformation, the hybrid domain swings out about 60°, resulting in a 70-Å displacement of the $\beta$-subunit knee away from the $\alpha$-subunit knee.

In the bent integrin conformation, the headpiece is in the closed conformation. After a switchblade-like extension at the integrin knees, the headpiece is found in both closed and open conformations (2). Extensive interfaces between the integrin headpiece and lower legs in the bent conformation are broken both by integrin extension and by hybrid domain swing-out; therefore, headpiece opening is less energetically costly in the extended than in the bent conformation. Conversely, headpiece opening favors integrin extension. This provides a mechanism in integrins for communicating activation signals between the ligand binding site in the headpiece and cytoskeletal protein-binding sites in the $\alpha$ and $\beta$-subunit cytoplasmic domains.

Characterization of integrin variants has provided strong evidence linking the "open" state observed in crystal structures, the "extended" integrin morphology observed via negative staining electron microscopy, and the "high affinity for ligand" state observed in cell adhesion assays. One such study introduced an *N*-glycosylation site at the most acute region of the

[5] The abbreviations used are: MIDAS, metal ion-dependent adhesion site; SASA, solvent-accessible surface area; CHO, Chinese hamster ovary; mAb, monoclonal antibody; FITC, fluorescein isothiocyanate; MFI, mean fluorescence intensity; LIBS, ligand-induced binding site.
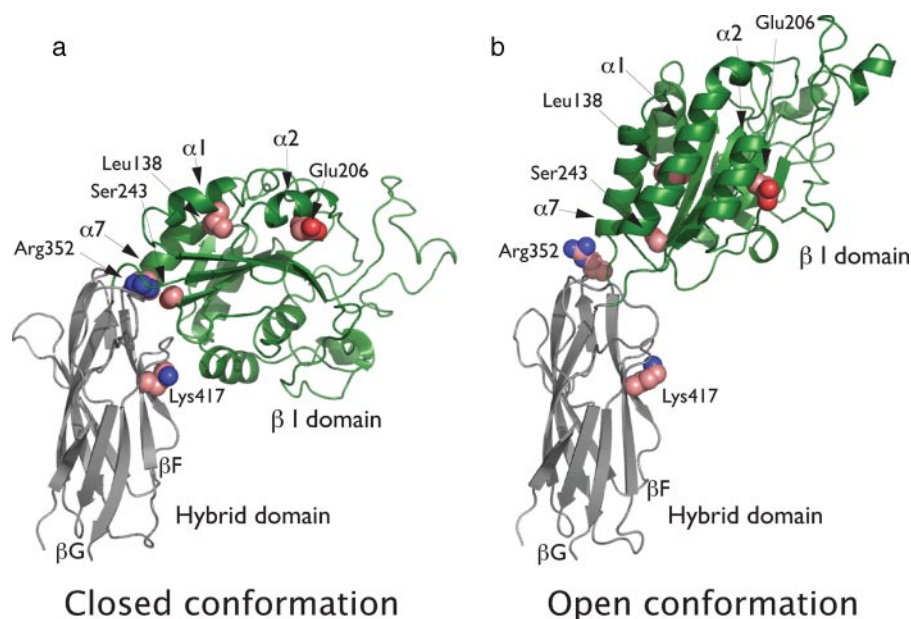
FIGURE 1. **An overview of the integrin αIIbβ3 conformational change, showing the closed (*a*) and open (*b*) conformations.** Structures are aligned using the hybrid domain, and sites of mutated residues are shown in a *space fill representation*. This figure was generated using PyMOL (14).

residues in the open state were taken as the median from values computed using each of six αIIbβ3 structures: Protein Data Bank codes 1txv, 1ty3, 1ty5, 1ty6, 1ty7, and 1tye (8). In all cases, the range of residues considered was Pro[57]–Asp[432]. After the mutational studies were completed, five of these open structures were rerefined, and four further ones were reported: Protein Data Bank codes 2vc2, 2vdk, 2vdl, 2vdm, 2vdn, 2vdo, 2vdp, 2vdq, and 2vdr (13). Moreover, a higher resolution and better refined closed structure of αIIbβ3 was reported.[6] The environment of each selected residue was computed retrospectively for these structures as well, by using only the newer or rerefined structures. For cases in which more than one subunit was present in the asymmetric unit, calculations were averaged over all independent subunits. This retrospective analysis shows no qualitative differences to the data collected using the smaller set of structures (Table 1), except for the quality of packing around Leu[138] and Glu[206] (the new open αIIbβ3 structures exhibit better packing at these positions than the new closed structures). The electron density around these two residue environments is not well resolved in the newer closed structures, however, which may explain these differences. Pro[85] was originally selected as a site for mutation but has been discarded from the current study because it was assigned as *cis* in open αIIbβ3 and *trans* in closed αVβ3 but subsequently *cis* in closed αIIbβ3; furthermore, the mutation of this *cis*-Pro to Gly resulted in a lack of expression (data not shown). The side chain solvent-accessible surface area (SASA) was computed using a 1.4-Å probe to search for sites buried in the closed state but exposed in the open state.

The quality of packing of each residue was additionally assessed via "SASApack." This measure involves computing the side chain-accessible surface area using a 0.5-Å probe and comparing the value to the average value for side chains with similar SASA (computed using a 1.4-Å probe). This metric has proven effective at detecting packing defects, since holes lead to an increase in the accessible surface area available to a small probe.[7]

*Plasmid Construction, Expression, and Immunoprecipitation*—Plasmids coding for full-length human αIIb and β3 were subcloned into pEF/V5-HisA and pcDNA3.1/Myc-His (+), respectively (5). Single-residue substitutions of β3 were carried out using site-directed mutagenesis. Constructs were transfected into CHO-K1 cells (American Type Culture Collection) using a Fugene transfection kit (Roche Applied Science) according to

interface between the β I domain and the hybrid domain. The resulting glycan "wedge," designed to shift the conformational balance toward the open state, was indeed found to increase ligand binding affinity (9, 10). This study laid the groundwork for understanding the relationship of the hinge between the β I domain and the hybrid domain to ligand binding affinity.

Here, we seek to extend the understanding of integrin function beyond the resolution afforded by the glycan wedge. We test the hypothesis that the detailed interactions that differ between crystal structures in the open and closed headpiece conformations indeed form the basis for allosteric regulation of ligand binding affinity and that shifting the equilibrium toward the open headpiece also shifts the equilibrium from the bent toward the extended conformation. Protein engineering can manipulate the energetic balance between alternate conformational states of proteins (11). We have applied computational design techniques to select single amino acid side chains that play an important role in the energetic balance between the open and closed conformations of αIIbβ3. A series of single-point mutants was rationally designed, with the goal of stabilizing the open conformation of αIIbβ3 relative to the closed conformation. These mutations were predicted to enhance both ligand binding affinity and integrin extension on the cell surface.

## MATERIALS AND METHODS

*Identification of Sites for Mutation*—Identification of sites for mutation was carried out by using the Rosetta software package to compute differences in the environment of each residue associated with the switch between the open and closed conformations. The residue environments for residues in the closed state were taken as the median from values computed using each of four αvβ3 structures: Protein Data Bank codes 1jv2, 1l5g, 1m1x, and 1u8c (3, 4, 12). The residue environments for

[6] Zhu, J., Luo, B. H., Xiao, T., Zhang, C., Nishida, N., and Springer, T. A. (2008) *Mol. Cell* **32,** 849–861.

[7] P. Bradley, personal communication.

**TABLE 1**

**Median value of quantifiers computed from multiple Protein Data Bank structures for the open and closed states**

Values are shown separately for structures available at the time the mutants were designed (on the left), and for structures released subsequently (on the right). Italicized values formed the basis for designed mutants.

| Quantifier | Open state structures used in designing mutants (6) | Closed state structures used in designing mutants (4) | Current open state structures (9) | Current closed state structures (5) |
|---|---|---|---|---|
| SASA (Å²) | Leu[138]: 0.0<br>Glu[206]: 47.3<br>*Ser[243]: 41.4*<br>*Arg[352]: 99.9*<br>*Lys[417]: 38.0* | Leu[138]: 1.3<br>Glu[206]: 26.7<br>*Ser[243]: 9.1*<br>*Arg[352]: 2.7*<br>*Lys[417]: 9.4* | Leu[138]: 0.0<br>Glu[206]: 53.1<br>Ser[243]: 39.4<br>Arg[352]: 102.3<br>Lys[417]: 33.7 | Leu[138]: 1.7<br>Glu[206]: 25.0<br>Ser[243]: 6.6<br>Arg[352]: 3.7<br>Lys[417]: 10.7 |
| SASApack (dimensionless) | *Leu[138]: 9.7*<br>*Glu[206]: 4.1*<br>Ser[243]: 2.5<br>Arg[352]: −0.3<br>Lys[417]: −0.8 | *Leu[138]: 0.0*<br>*Glu[206]: 1.5*<br>Ser[243]: 10.2<br>Arg[352]: 5.0<br>Lys[417]: −2.9 | Leu[138]: 3.65<br>Glu[206]: −0.87<br>Ser[243]: 2.13<br>Arg[352]: 0.22<br>Lys[417]: 8.42 | Leu[138]: 0.3<br>Glu[206]: 1.5<br>Ser[243]: 10.2<br>Arg[352]: 7.3<br>Lys[417]: 1.0 |

the manufacturer's instructions. Stably transfected CHO cells were established as described (9). The expression levels of αIIb and β3 were detected by flow cytometry staining with the following monoclonal antibodies: 10E5 (anti-αIIb mAb, kindly provided by B. S. Coller, The Rockefeller University, New York, NY) (15), 7E3 (anti-β3 mAb), and AP3 (nonfunctional anti-β3 mAb, American Type Culture Collection), respectively.

*Soluble Ligand Binding*—The activating anti-αIIb mAb PT25-2 was a generous gift from M. Handa (Keio University Hospital, Tokyo, Japan) (16). Soluble binding of FITC-labeled human fibrinogen (Enzyme Research Laboratories, South Bend, IN) and ligand mimetic IgM PAC-1 (BD Biosciences) was determined as described (9). Briefly, transfected cells suspended in 20 mM Hepes-buffered saline (pH 7.4) supplemented with 5.5 mM glucose and 1% bovine serum albumin were incubated with FITC-conjugated human fibrinogen or PAC-1 in the presence of either 5 mM EDTA; 1 mM $Ca^{2+}$, 1 mM $Mg^{2+}$, 1 mM $Mn^{2+}$; 1 mM $Ca^{2+}$, 1 mM $Mg^{2+}$ plus 10 μg/ml activating mAb PT25-2; or 1 mM $Mn^{2+}$ plus 10 μg/ml PT25-2 at room temperature for 30 min. For PAC-1 binding, cells were washed and stained with FITC-conjugated anti-mouse IgM on ice for another 30 min before being subjected to flow cytometry. Cells were also stained in parallel with anti-β3 mAb AP3 followed by FITC-conjugated anti-mouse IgG. Binding activity is presented as the percentage of the mean fluorescence intensity (MFI) of PAC-1 or fibrinogen staining, after background subtraction of the staining in the presence of EDTA, relative to the MFI of the AP3 staining.

*Cell Adhesion*—Cell adhesion on immobilized human fibrinogen was assayed using cellular lactate dehydrogenase (17). Briefly, cells suspended in Hepes-buffered saline supplemented with 5.5 mM glucose and 1% bovine serum albumin and either 1 mM EDTA or 1 mM $Ca^{2+}$ plus 1 mM $Mg^{2+}$ were added to flat bottom 96-well plates ($1 \times 10^4$ cells/well) that had been precoated with different concentrations of fibrinogen and blocked with 1% bovine serum albumin. After incubation at 37 °C for 1 h, wells were washed three times with Hepes-buffered saline supplemented as indicated above. Remaining adherent cells were lysed with 1% Triton X-100, and lactate dehydrogenase activity was assayed using the Cytotoxicity Detection Kit (LDH) (Roche Applied Science) according to the manufacturer's instructions.

*Ligand-induced Binding Site (LIBS) Epitope Expression*—Anti-LIBS mAb AP5, LIBS1, and D3 were kindly provided by M. H.

Ginsberg (University of California San Diego, La Jolla, CA) and L. K. Jennings (University of Tennessee Health Science Center, Memphis, TN). LIBS epitope expression was determined as described previously (9). In brief, transfected cells suspended in Hepes-buffered saline supplemented with 5.5 mM glucose and 1% bovine serum albumin were incubated with or without 50 μM Gly-Arg-Gly-Asp-Ser-Pro peptide (GRGDSP) in the presence of 1 mM $Ca^{2+}$ plus 1 mM $Mg^{2+}$ and 10 μg/ml anti-LIBS antibodies or control X63 IgG. After incubation at room temperature for 30 min, cells were washed and stained with FITC-labeled anti-mouse IgG on ice for 30 min. The stained cells were subjected to flow cytometry, and LIBS epitope expression was expressed as the percentage of MFI of anti-LIBS antibody after subtraction of MFI of the control X63 IgG, relative to MFI of the conformation-independent anti-β3 mAb AP3 after subtraction of the same control.

## RESULTS

*Rationale for Mutations to Stabilize β3 Integrin in the Open State*—Initally, conventional computational design methodologies (18) were applied to collect a series of mutations predicted to be stabilizing for each of several open β3 state integrin structures. Incorporation of a predicted stabilizing mutation from one open state structure onto a different open state structure, however, seldom proved stabilizing; this was an indication that the design methodology was too sensitive to structural details to be useful for this application. For this reason, mutations at each site were selected as per the rationale described below.

Computational design was based on multiple examples of β3 integrin structures in each of the closed and open conformations (Table 1). Changes in residue environments as measured by SASA or SASApack (see "Materials and Methods") between closed and open structures were used to identify sites of mutation. Due to the moderate resolution of the crystal structures used (Bragg spacings for these structures range from 2.7 to 3.3 Å), emphasis was placed on disruption of specific stabilizing interactions in the closed conformation rather than design of new stabilizing interactions in the open conformation. Residues near the fibrinogen-binding site were not considered.

*Arg[352] (β I-Hybrid Interface)*—The solvent-accessible surface area of Arg[352] increases considerably in switching from the closed to the open state (Table 1). At the C-terminal end of the α7-helix of the β I domain, Arg[352] appears to play a critical role in stabilizing the closed state, in which it is fully
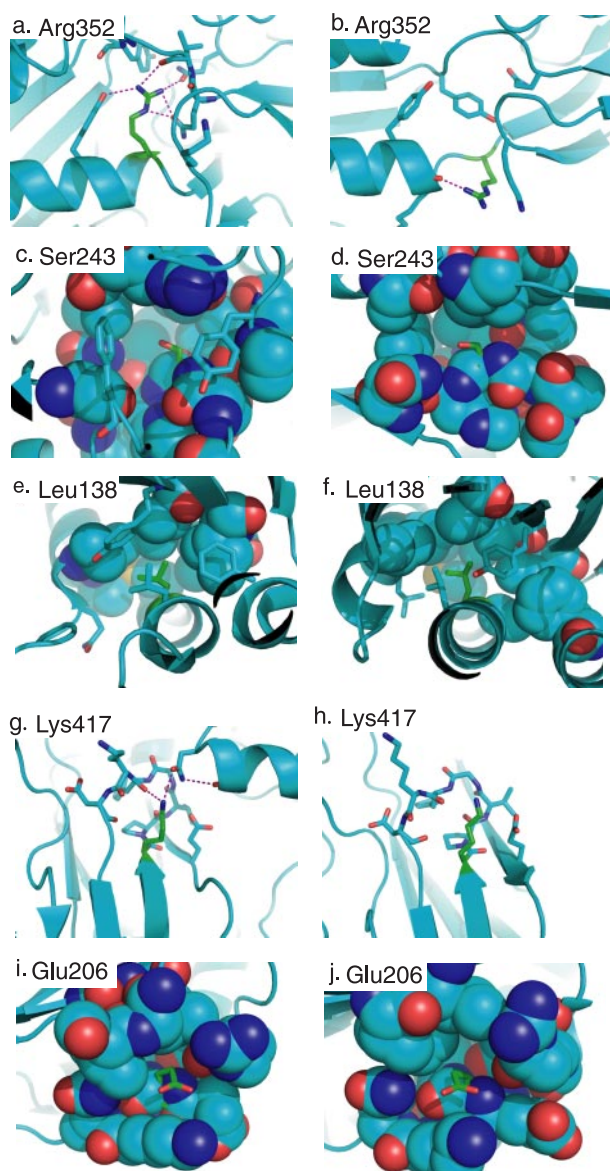
## Closed conformation  Open conformation



FIGURE 2. **A detailed examination of the environment of each mutated residue, in the closed (*a, c, e, g,* and *i*) and open (*b, d, f, h,* and *j*) conformations.** Mutated residues were as follows: Arg[352] (*a* and *b*), Ser[243] (*c* and *d*), Leu[138] (*e* and *f*), Lys[417] (*g* and *h*), and Glu[206] (*i* and *j*). This figure was generated using PyMOL (14).

occluded from solvent and forms a series of hydrogen bonds (Fig. 2*a*). After the switch to the open state, however, the α7-helix unwinds just enough that this side chain becomes largely exposed and forms a single surface-exposed hydrogen bond that caps the C terminus of the α7-helix (Fig. 2*b*). In order to destabilize the closed state with minimal disruption of the open state, a glutamate was introduced at this position.

*Ser²⁴³ (β I-Hybrid Interface)*—The solvent-accessible surface area of this side chain near the hinge region was also found to increase upon switching from the closed to open state (Table 1). In the closed state, this partially buried serine side chain faces the α7-helix and occupies a small cavity below the plane of the side chain of Arg[352] (described above) (Fig. 2*c*). This cavity is sterically bounded by Tyr[110] and Phe[421], shown in the *fore-*

*ground* of Fig. 2*c* (in *stick representation*). The relocation of the α7-helix and release of Arg[352] associated with the transition to the open conformation, meanwhile, expose this side chain to solvent (Fig. 2*d*). Additionally, Tyr[110] and Phe[421] have shifted to where they are no longer visible in the view presented (Fig. 2*d*). In order to take advantage of the tight steric constraints of the low affinity state, aspartate and glutamate were each introduced in place of this serine.

*Leu¹³⁸ (β I Domain)*—The SASApack value computed for this leucine side chain in the closed conformation, about zero, showed that this residue was packed in an environment similar to that of an average leucine in the Protein Data Bank (Table 1). After the transition to the open conformation, however, this side chain was much less well packed than the Protein Data Bank average for leucine (Table 1). Examination of the surrounding side chains shows that packing considerations are responsible for this difference. In the closed state, this inward facing leucine side chain fits snugly into a pocket that exactly complements the shape of the side chain (Fig. 2*e*). Upon transition to the open conformation, however, the α1-helix slides relative to the rest of the β I domain, such that this side chain fits into a pocket formed by a different set of side chains. This pocket exhibits much less shape complementarity toward the leucine side chain (Fig. 2*f*); in particular, a void remains near the leucine C-β atom, which would be filled by substitution of a β-branched amino acid at this position. To improve the packing of the open conformation while disrupting the packing of the closed conformation, this position was mutated to isoleucine.

*Lys⁴¹⁷ (Hybrid Domain)*—A difference in SASA between the open and closed conformations was observed for this lysine side chain (Table 1), which is located on the outward facing side of the βF-strand of the hybrid domain. In the closed state, the βF-βG loop adopts a noncanonical conformation, allowing it to pack against the α5-helix of the β I domain. The backbone carbonyl groups in this loop face inward, allowing one of these to form a hydrogen bond to the side chain of Lys[417]. This lysine side chain also forms a hydrogen bond to Asn[303], which in turn acts as a "capping residue" on the C-terminal end of the α5-helix (Fig. 2*g*).

The hinge motion involved in the transition to the open conformation results in a complete loss of the interactions between the βF-βG loop and the β I domain, exposing the outward facing side chains on the βF-strand of the hybrid domain (including Lys[417]). The conformation of the βF-βG loop relaxes, allowing the backbone to form hydrogen bonds to solvent (Fig. 2*h*). Given the relative unimportance of the detailed interactions in the open conformation (further supported by the higher crystallographic B-factors in this state), "charge reversal" mutations of Lys[417] to aspartate and glutamate were introduced to disrupt the hydrogen bonds stabilizing the βF-βG loop in the closed conformation.

*Glu²⁰⁶ (β I Domain)*—Although the most obvious structural rearrangement of the β I domain takes place in the α1- and α7-helices, a very subtle twist occurs in the α2-helix as well (8). Comparison of the quality of packing in both states via SASA-pack (see "Materials and Methods") brought to light a subtle difference in this region (Table 1).
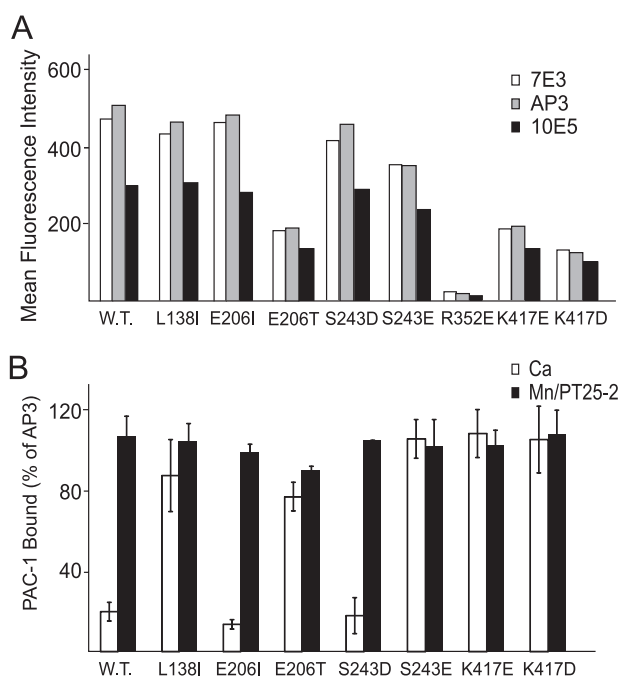
FIGURE 3. **Expression and soluble ligand binding of integrin αIIbβ3 on 293T cells.** *A*, 293T transient transfectants were immunofluorescently stained with mAbs 7E3 (*open bars*), AP3 (*gray bars*), and 10E5 (*black bars*). *B*, soluble PAC-1 binding to 293T transfectants was determined in the presence of 5 mM $Ca^{2+}$ (*open bars*) or 1 mM $Mn^{2+}$ plus 10 μg/ml mAb PT25-2 (*black bars*) and is expressed as the MFI of PAC-1 staining as a percentage of MFI of staining with AP3. Data are mean and S.D. of three independent experiments.

Although the aliphatic portion of the $Glu^{206}$ side chain packs snugly against $Val^{193}$ and $Leu^{194}$ in the closed conformation (Fig. 2*i*), this interaction is lost in the open conformation (Fig. 2*j*). This small decrease in packing density led to the hypothesis that introduction of a β-branched amino acid in place of this glutamate could be accommodated in the open conformation but would prove greatly destabilizing to the closed conformation. Mutations to isoleucine and threonine were therefore introduced in place of this glutamate.

In all, eight point mutants were selected at five sites: R352E, S243D, S243E, L138I, K417D, K417E, E206I, and E206T. As shown in Fig. 1, these sites are not restricted to the hinge region connecting the β I and hybrid domains; rather, they span the pathway that transmits the conformational change from the cell surface to the fibrinogen-binding site. Each of these point mutations was tested independently to gauge its effect on expression and ligand binding.

*Expression of the Mutant αIIbβ3 in 293T Cells*—To determine whether these mutant β3 integrins could be expressed with the αIIb-subunit, we transiently transfected the eight αIIbβ3 mutants into 293T cells. Two anti-β3 antibodies, 7E3 and AP3, and an αβ complex-dependent anti-αIIb antibody, 10E5, were used to monitor expression on the cell surface. All three antibodies gave similar results (Fig. 3*A*). Three mutants (L138I, E206I, and S243D) were expressed at wild-type levels. Four mutants (E206T, S243E, K417E, and K417D) were expressed at levels lower than that of the wild type. The remaining mutant, R352E, was not expressed at detectable levels.

*Five Mutants Have Enhanced Ligand Binding Affinity*—The seven expressed mutants were tested for ligand binding in 293T

transfectants. In all experiments measuring binding of the ligand-mimetic antibody PAC-1 or soluble fibrinogen, binding was expressed relative to αIIbβ3 surface expression to correct for differing amounts of cell surface expression by the mutants. In the presence of $Ca^{2+}$, wild type αIIbβ3 bound very little ligand-mimetic PAC-1 antibody, whereas the presence of $Mn^{2+}$ and activating mAb PT25-2 greatly increased binding (Fig. 3*B*). In contrast to wild type, five of the seven mutants, L138I, E206T, S243E, K417E, and K417D, bound PAC-1 in $Ca^{2+}$ (Fig. 3*B*). Binding in $Ca^{2+}$ was comparable with that in activating conditions and with activated wild-type.

We have previously observed that mutations that stabilize integrins in the high affinity, extended conformation lead to decreased cell surface expression, presumably because the bent conformation is more efficiently processed and transported to the cell surface (9). Consistent with the tendency of activating mutations to decrease surface expression, three of five activating mutations, E206T, K417E, and K417D, decreased surface expression, whereas the two nonactivating mutations, E206I and S243D, had no effect on surface expression (Fig. 3). However, the L138I and S243E mutations were activating while having no or little effect on surface expression.

To further characterize the five high affinity mutants, stable CHO-K1 cell transfectants were established, and clones with similar expression of wild-type and mutant αIIbβ3 were selected. Soluble PAC-1 (Fig. 4*A*) and fibrinogen (Fig. 4*B*) binding showed that wild type αIIbβ3 bound ligands only when stimulated by $Mn^{2+}$ and/or PT25-2. By contrast, the five mutants bound ligands with significant higher capability in the presence of $Ca^2$, confirming that all five mutations activated integrins for ligand binding (Fig. 4, *A* and *B*). In the presence of $Mn^{2+}$ and PT25-2, all mutations and wild-type bound ligands maximally.

The affinity state of the wild type and mutants was further assessed by cell adhesion assays on immobilized fibrinogen. In contrast to soluble ligand binding, at coating concentrations above 5 μg/ml, wild type cells mediated efficient adhesion to immobilized fibrinogen even in the absence of activation (Fig. 4*C*). All mutant cells adhered to immobilized fibrinogen at lower coating concentrations than wild-type, and two mutants, K417E and K417D, even adhered to the substrate at 1 μg/ml coating concentrations.

*Mutations That Enhanced Ligand Binding Stabilized Integrins in the Extended Conformation*—Activation and/or ligand binding change the conformation of αIIbβ3, resulting in the exposure of neoepitopes called LIBS. We investigated the conformation of the mutants with three different LIBS antibodies, which bind to various sites in the β3-subunit (Fig. 5). Under basal conditions in $Ca^{2+}$, all mutants showed increased expression of the D3 (anti-β3 residues 422–490) (19) and LIBS1 (anti-β3 residues 422–690) (20) epitopes and, with the exception of S243E, showed increased expression of the AP5 (anti-β3 residues 1–5) (20) epitope. Thus, the equilibrium is shifted to a more extended conformation in the five mutant receptors with higher affinity for ligand.
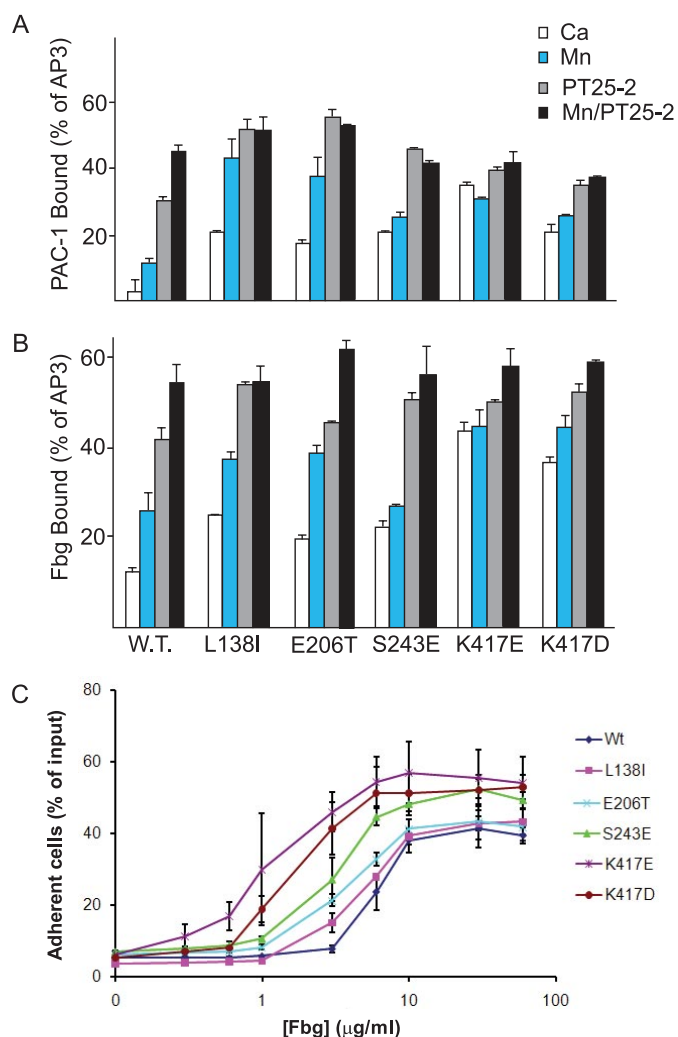
FIGURE 4. **Ligand binding activity of integrin αIIbβ3 on CHO-K1 cells.** *A* and *B*, soluble ligand binding. Cells were incubated with PAC-1 (*A*) or FITC-fibrinogen (*B*) in different conditions, as shown in the figures and determined as described under "Materials and Methods." *C*, adhesion of the wild type and mutant transfectants to surface coated with fibrinogen at the indicated concentrations. Data are representative of three independent experiments, each in duplicate or triplicate. The representative experiment shown was in triplicate, and bars show S.D.



FIGURE 5. **Exposure of LIBS epitopes.** Wild type and mutant αIIbβ3 CHO cell transfectants were incubated with LIBS mAbs AP5 (*A*), D3 (*B*), and LIBS1 (*C*) in the presence of 5 mM Ca$^{2+}$ (*open bars*) or 1 mM Mn2$^+$ plus 100 μM GRGDSP peptide (*black bars*) as described under "Materials and Methods." Consistent results were obtained in three independent experiments done in singlicate, with two experiments on CHO transfectants as shown (mean and difference from mean) and one on 293T transfectants.

## DISCUSSION

We computationally designed mutations that energetically favor the open, high affinity conformation of the β3 integrin headpiece. Five of the eight designed mutations bound ligands much better than wild type. More interestingly, these mutants were found to be in the more extended conformation than wild type, suggesting that the conformational change at the ligand binding headpiece was propagated to the legs of the integrin.

*Rationalization of Unsuccessful Mutations*—As noted earlier, locking the integrins into the open conformation through the introduction of a glycan wedge in the interface region led to a significant decrease in expression levels (9). It is therefore not entirely surprising that one of the mutations that may be expected to most destabilize the closed conformation (R352E) essentially abolished expression.

Unlike this unsuccessful design, however, two of the mutants, S243D and E206I, were expressed but failed to show a significant increase of ligand binding capability. For-
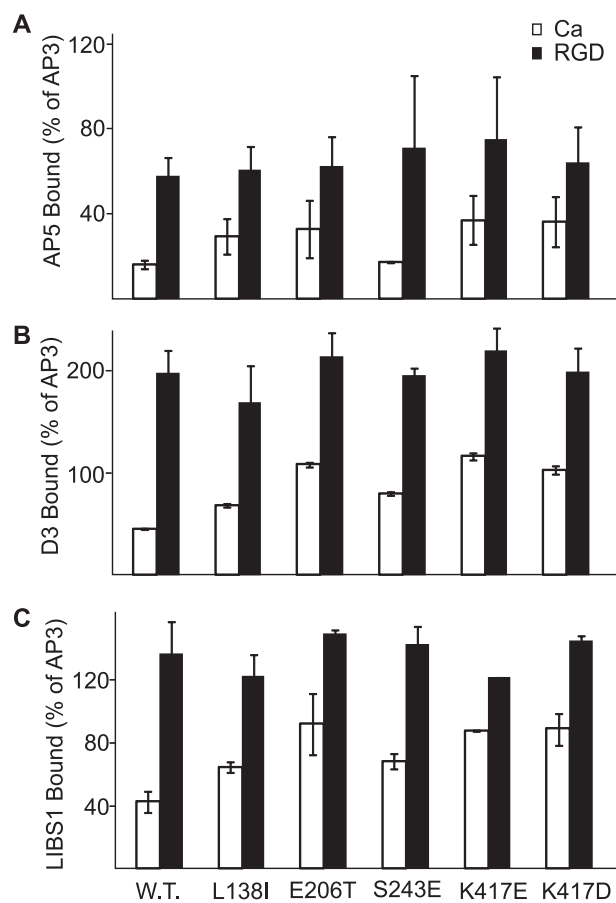
tuitously, another mutation tested at each of these sites showed increased ligand-binding; this allows for a direct retrospective comparison.

In the case of substitutions at Ser[243], RosettaDesign (21) was used to build both Asp and Glu side chains at this position of each crystal structure, keeping the backbones fixed. Examination of these structural models (Fig. 6) suggests an explanation for the different behavior of these two mutants.

In the closed conformation, both Asp and Glu may be sterically accommodated in place of Ser[243]; in both cases, however, the geometry of the substituted side chain is not suitable to form a hydrogen bond, leaving this charged group unsatisfied (Fig. 6, *a* and *c*). The models of the open conformation, however, show a marked difference between Asp and Glu. Although the aliphatic part of the glutamate side chain is long enough that the carboxyl group may be fully exposed to solvent (Fig. 6*b*), this is not true of the aspartate side chain; the Asp side chain is buried by its environment in a manner that precludes formation of a hydrogen bond in the open conformation (Fig. 6*d*).

Based on these models, we therefore conclude that introduction of the S243D mutation destabilizes both the open and closed conformations to a similar extent, leading to ligand affinity comparable with that of the wild type. By contrast, S243E
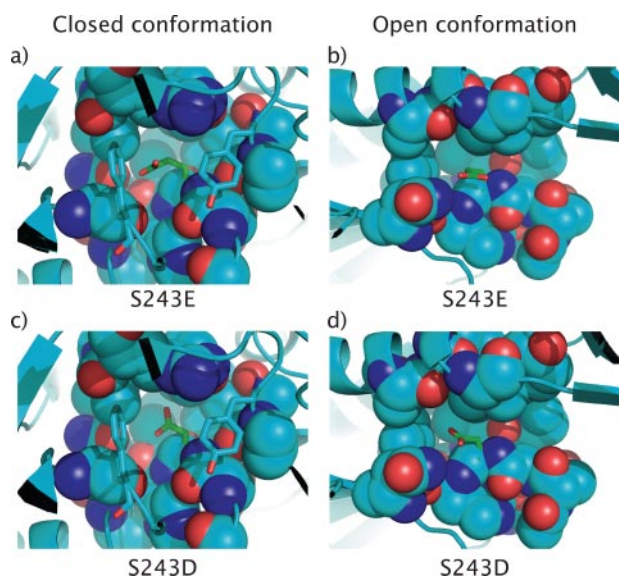
Closed conformation    Open conformation

a)          b)

S243E       S243E

c)          d)

S243D       S243D

FIGURE 6. **Comparison of structural models of the S243E (*a* and *b*) and S243D (*c* and *d*) mutants, in the closed conformation (*a* and *c*) and in the open conformation (*b* and *d*), built using RosettaDesign.** This figure was generated using PyMOL (14).

destabilizes only the closed conformation, leading to an increase in ligand binding affinity.

A similar structural explanation may underlie the difference in the observed behavior of the E206I and E206T mutants. Although the E206T mutant demonstrates that disruption at this site is indeed a viable method for enhancing ligand binding affinity, isoleucine was not a good choice at this position. The energetic details underlying the differences between E206I and E206T are more complex, however, stemming from the chemical as well as steric differences between isoleucine and threonine.

*Strategy for Selection of Mutation Sites*—Although not all of the mutations led to the desired increase in ligand binding affinity, each site identified from the computational comparison led to at least one mutant with altered behavior. This underscores the robustness of the strategy of selecting mutation sites based on differences in SASA and packing. This robust approach was developed specifically to cater to this design problem because of the relatively poor resolution of crystal structures of each state (Bragg spacings for the structures of the closed conformation range from 3.1 to 3.3 Å and from 2.7 to 3.1 Å for the structures of the open conformation). This had two implications in selecting a design strategy.

First, it has long been known that crystal structures of poor resolution suffer larger deviations in torsion angles (22) as well as irregular packing (23). Since both of these features are captured in the full RosettaDesign energy function (21), it was not clear that residues scoring poorly with this energy function were indeed subject to energetic strain; rather, observed differences between the two conformations could be due solely to slight inaccuracies in atomic positions. For this reason, assessment of residue environments focused on using features that would be more robust toward such inaccuracies, such as solvent-accessible surface area. The use of six structures to represent the open conformation was an additional measure to alleviate these concerns.

Whereas the possible design strategy of relieving strain specific to the open conformation did not seem promising, a related approach, designing new favorable interactions specific to the open conformation, might also be expected to fail for the same reasons. Such an approach has recently been used in the thermostabilization of an enzyme (18), demonstrating that function can be maintained after incorporation of new stabilizing interactions, but the structure of the target protein used in this study was available at a resolution of 1.14 Å (24).

Here, we have demonstrated that crystal structures at about 3 Å resolution are sufficient for rationally designing mutations that will preferentially destabilize one conformation, by using "robust" measures to select sites for mutation. This, in turn, raises the interesting possibility of using high quality homology models as the basis for selecting sites for mutation. The usefulness as a search model for solving the crystallographic "phase problem" via molecular replacement represents a very stringent test of the accuracy of a homology model (25). Recent progress in structure prediction has greatly loosened the requirement of sequence similarity for building models of sufficient accuracy for molecular replacement (26). This, together with design strategies that specifically focus on yielding robust results from structures at relatively poor resolution, offers the tantalizing prospect for rational manipulation of protein states for which high quality crystal structures are not yet available.

*Mutational Studies of Mechanism of Allosteric Switch*—Interestingly, the five mutants with enhanced ligand binding affinity were found to be in a conformation more extended than wild type, suggesting that the conformational change at the ligand binding headpiece was propagated to the integrin legs. Previously, we showed that introducing a bulky glycan group to the interface between the β1 or β3 I domain and hybrid domain caused integrins to adopt a high affinity and extended conformation (9, 10). Other studies showed that mutations introduced in the β1 integrin I domain increased ligand binding and shifted the equilibrium toward more extended conformation (27). However, introducing disulfides to the β3 I domain C-terminal α7-helix or deleting four residues of the β2 I domain α7-helix increased integrin ligand binding, whereas the overall conformation of the receptors was still in the bent conformation unless ligands were added (28, 29), probably because these mutations circumvented allosteric communication of the β3 I domain through its α7-helix with the hybrid domain (30). Here, our studies demonstrate that single-residue substitutions both in the β3 I domain and in the hybrid domain can stabilize this integrin in the high affinity, extended conformation. The results suggest that integrins are pliable to environmental change; subtle changes in the structure, either by mutation or by binding of other proteins, can readily shift the equilibrium from one conformer to the other.

Preferential stabilization of one integrin conformation represents an attractive method for understanding integrin function; not surprisingly, several approaches have been used to engineer integrins locked into either the high or low affinity state.

Rationally designed amino acid substitutions have previously been applied to selectively stabilize both the open and closed states of a different integrin, Mac-1 (αMβ2, or CD11b/CD18).

Several single- and double-point mutants in the α-I domain have been described (31–33), which lead to modest increases in the ligand binding affinity (34). Much larger effects on ligand binding affinity were obtained through the complete computational redesign of the α-I domain core (35). By using crystal structures of the open and closed conformations of this domain, redesigned domains were proposed and tested. These redesigned domains, which required four mutations to stabilize the closed conformation and 8–13 mutations to stabilize the open conformation, induced a stronger shift toward the desired conformation than a single-point mutant included for comparison (35).

Although it is expected to be generally true that the complete redesign of a protein core is likely to induce a larger energetic shift than most single-point mutants, such an approach was not applied to αIIbβ3, for two reasons. First, the crystal structures of the Mac-1 α-I domain were available at better resolution than the structures of the β3 headpiece. Second, carefully chosen single-point mutants are more likely to preserve subtle details of the structure, which can be important for maintaining long range propagation of the conformational changes as well as binding surfaces for other proteins. Both of these are preserved in the series of mutations presented here, evidenced by binding of anti-LIBS antibodies and the fact that mutations in the hybrid domain affect ligand binding in the β I domain.

## CONCLUSIONS

Integrins represent attractive pharmaceutical targets for a variety of human diseases; abciximab, eptifibatide, and tirofiban all target integrin αIIbβ3 and have been approved by the United States Food and Drug Administration for the treatment of thrombosis (36, 37). Whereas these compounds block the interaction of integrins with the receptor, the conformational changes they induce can themselves initiate unwanted signals. In fact, it has been shown that these three antagonists can induce thrombocytopenia in 1–5% of patients (37). Due to the importance of allostery in regulating integrin function, it is critical to extend our detailed understanding of the relationship of integrin conformation with ligand binding.

## REFERENCES

1. Volkman, B. F., Lipson, D., Wemmer, D. E., and Kern, D. (2001) *Science* **291,** 2429–2433
2. Luo, B.-H., Carman, C. V., and Springer, T. A. (2007) *Annu. Rev. Immunol.* **25,** 619–647
3. Xiong, J.-P., Stehle, T., Diefenbach, B., Zhang, R., Dunker, R., Scott, D. L., Joachimiak, A., Goodman, S. L., and Arnaout, M. A. (2001) *Science* **294,** 339–345
4. Xiong, J. P., Stehle, T., Zhang, R., Joachimiak, A., Frech, M., Goodman, S. L., and Arnaout, M. A. (2002) *Science* **296,** 151–155
5. Takagi, J., Petre, B. M., Walz, T., and Springer, T. A. (2002) *Cell* **110,** 599–611
6. Takagi, J., Strokovich, K., Springer, T. A., and Walz, T. (2003) *EMBO J.* **22,** 4607–4615
7. Kim, M., Carman, C. V., and Springer, T. A. (2003) *Science* **301,** 1720–1725
8. Xiao, T., Takagi, J., Wang, J.-h., Coller, B. S., and Springer, T. A. (2004) *Nature* **432,** 59–67
9. Luo, B.-H., Springer, T. A., and Takagi, J. (2003) *Proc. Natl. Acad. Sci. U. S. A.* **100,** 2403–2408
10. Luo, B.-H., Strokovich, K., Walz, T., Springer, T. A., and Takagi, J. (2004) *J. Biol. Chem.* **279,** 27466–27471
11. Ambroggio, X. I., and Kuhlman, B. (2006) *Curr. Opin. Struct. Biol.* **16,** 525–530
12. Xiong, J. P., Stehle, T., Goodman, S. L., and Arnaout, M. A. (2004) *J. Biol. Chem.* **279,** 40252–40254
13. Springer, T. A., Zhu, J., and Xiao, T. (2008) *J. Cell Biol.* **182,** 791–800
14. DeLano, W. L. (2004) *PyMol*, DeLano Scientific, San Carlos, CA
15. Coller, B. S., Peerschke, E. I., Scudder, L. E., and Sullivan, C. A. (1983) *J. Clin. Invest.* **72,** 325–338
16. Tokuhira, M., Handa, M., Kamata, T., Oda, A., Katayama, M., Tomiyama, Y., Murata, M., Kawai, Y., Watanabe, K., and Ikeda, Y. (1996) *Thromb. Haemost.* **76,** 1038–1046
17. Zhu, J., Carman, C. V., Kim, M., Shimaoka, M., Springer, T. A., and Luo, B.-H. (2007) *Blood* **110,** 2475–2483
18. Korkegian, A., Black, M. E., Baker, D., and Stoddard, B. L. (2005) *Science* **308,** 857–860
19. Kouns, W. C., Wall, C. D., White, M. M., Fox, C. F., and Jennings, L. K. (1990) *J. Biol. Chem.* **265,** 20594–20601
20. Honda, S., Tomiyama, Y., Pelletier, A. J., Annis, D., Honda, Y., Orchekowski, R., Ruggeri, Z., and Kunicki, T. J. (1995) *J. Biol. Chem.* **270,** 11947–11954
21. Kuhlman, B., Dantas, G., Ireton, G. C., Varani, G., Stoddard, B. L., and Baker, D. (2003) *Science* **302,** 1364–1368
22. Morris, A. L., MacArthur, M. W., Hutchinson, E. G., and Thornton, J. M. (1992) *Proteins* **12,** 345–364
23. Pontius, J., Richelle, J., and Wodak, S. J. (1996) *J. Mol. Biol.* **264,** 121–136
24. Ireton, G. C., Black, M. E., and Stoddard, B. L. (2003) *Structure* **11,** 961–972
25. Giorgetti, A., Raimondo, D., Miele, A. E., and Tramontano, A. (2005) *Bioinformatics* **21,** ii72–ii76
26. Qian, B., Raman, S., Das, R., Bradley, P., McCoy, A. J., Read, R. J., and Baker, D. (2007) *Nature* **450,** 259–267
27. Mould, A. P., Barton, S. J., Askari, J. A., McEwan, P. A., Buckley, P. A., Craig, S. E., and Humphries, M. J. (2003) *J. Biol. Chem.* **278,** 17028–17035
28. Luo, B.-H., Takagi, J., and Springer, T. A. (2004) *J. Biol. Chem.* **279,** 10215–10221
29. Yang, W., Shimaoka, M., Chen, J. F., and Springer, T. A. (2004) *Proc. Natl. Acad. Sci. U. S. A.* **101,** 2333–2338
30. Luo, B.-H., and Springer, T. A. (2006) *Curr. Opin. Cell Biol.* **18,** 579–586
31. Li, R., Rieu, P., Griffith, D. L., Scott, D., and Arnaout, M. A. (1998) *J. Cell Biol.* **143,** 1523–1534
32. Oxvig, C., Lu, C., and Springer, T. A. (1999) *Proc. Natl. Acad. Sci. U. S. A.* **96,** 2215–2220
33. Xiong, J.-P., Li, R., Essafi, M., Stehle, T., and Arnaout, M. A. (2000) *J. Biol. Chem.* **275,** 38762–38767
34. McCleverty, C. J., and Liddington, R. C. (2003) *Biochem. J.* **372,** 121–127
35. Shimaoka, M., Shifman, J. M., Jing, H., Takagi, J., Mayo, S. L., and Springer, T. A. (2000) *Nat. Struct. Biol.* **7,** 674–678
36. Coller, B. S. (2001) *Thromb. Haemost.* **86,** 427–443
37. Bennett, J. S. (2001) *Annu. Rev. Med.* **52,** 161–184